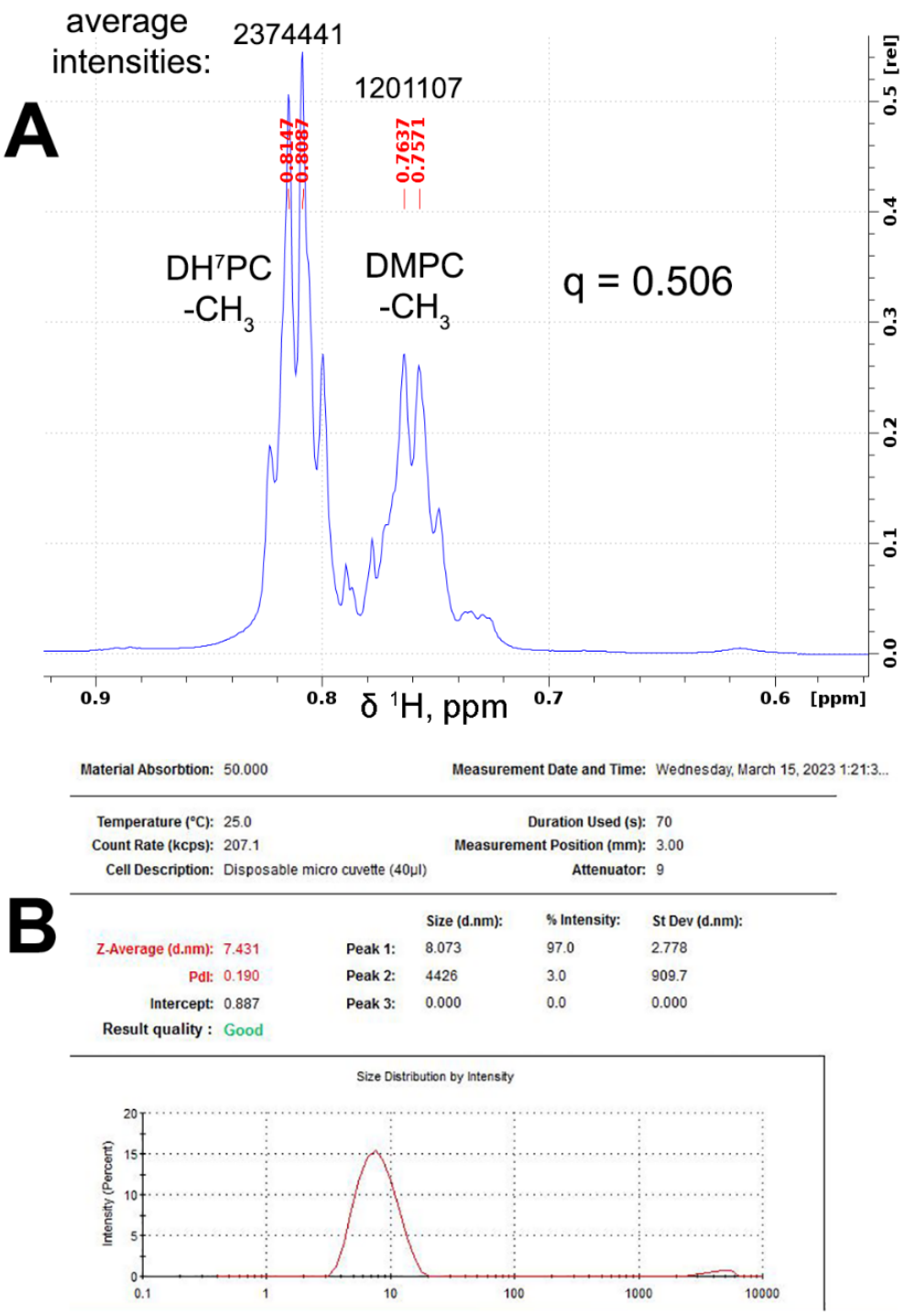

Figure S1. Composition and hydrodynamics of the DH^{7}PC:DMPC bicelles used. Related to Fig. 2. (A) The ratio of methyl NMR peak heights of 0.506 DMPC per DH^{7}PC is consistent with mixing of one and two molar equivalents, respectively. (B) Dynamic light scattering finds the mixtures to be dominated by particles with diameters of 8.1 to 8.2 nm.

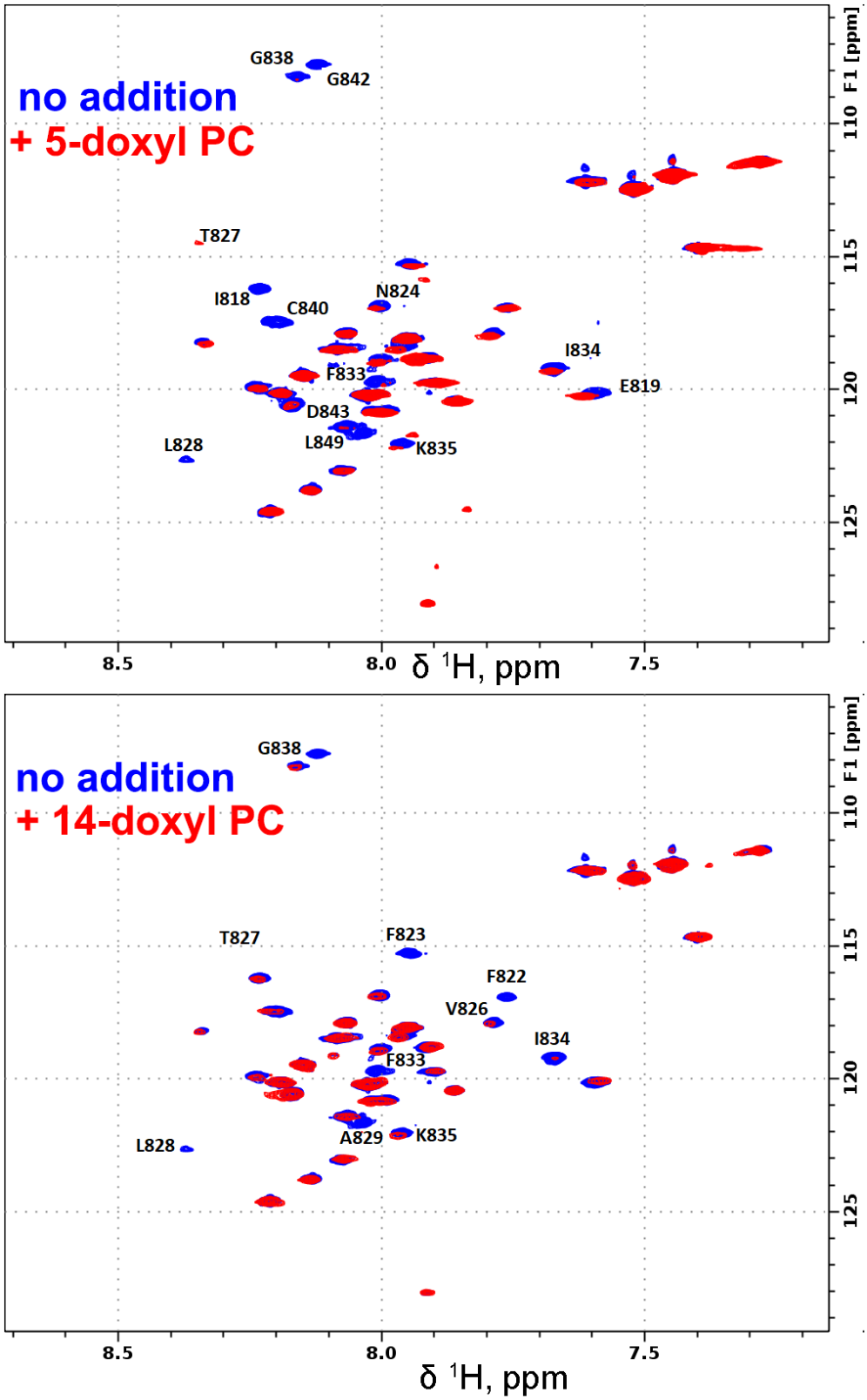

Figure S2. HSQC-CPMG spectra of FP in DMPC:DH^{7}PC bicelles at pH, 5 before and after adding a nitroxide spin-labeled phosphatidylcholine to about one per leaflet. Related to Fig. 2. Amide NMR peaks broadened by the spin-labeled lipid probe are labeled. To enhance the line broadening, the spectra have 8 ms of ^{1}H relaxation during the PROJECT-CPMG period of the pulse sequence.

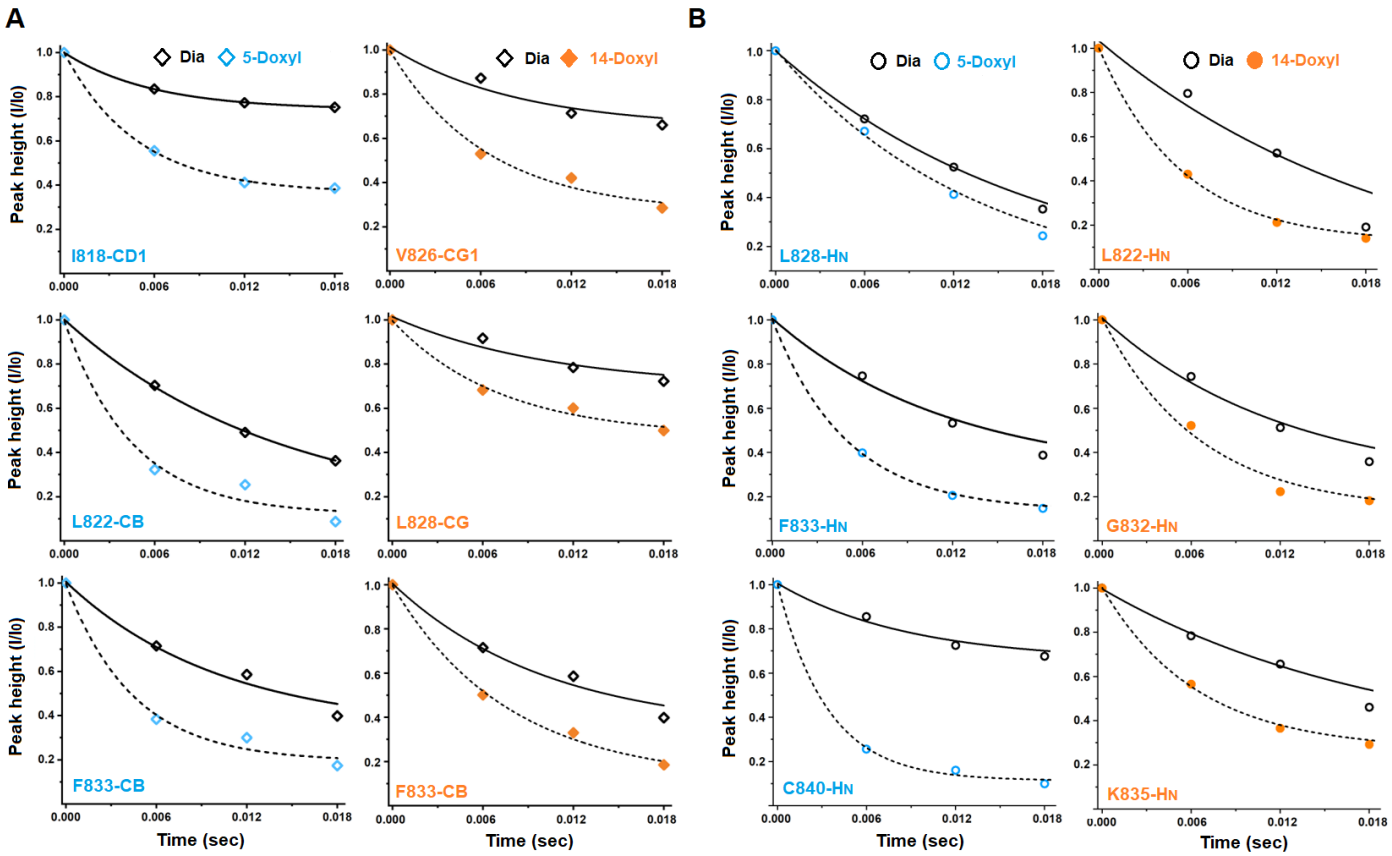

Figure S3: Examples of ^{1}H NMR relaxation with exponential fits used to quantify paramagnetic relaxation enhancements (PREs) as Γ_2 relaxation rate constants. Related to Fig. 2. Examples of ^{1}H NMR relaxation are plotted in the absence (black symbols and solid lines; diamagnetic reference) and the presence of nitroxide spin-labeled phosphatidylcholine (colored symbols and dashed lines; paramagnetic) at around one per leaflet. The presence of 16:0–5-doxyl PC is denoted by blue symbols. The presence of 16:0–14-doxyl PC is denoted by orange symbols. (A) Examples of ^{13}C-resolved methyl and methylene ^{1}H NMR relaxation (diamonds) are plotted, with exposure to 16:0–5-doxyl PC at left (blue) or 16:0-14-doxyl PC at right (orange). (B) Examples of ^{15}N-resolved amide ^{1}H NMR relaxation (circles) are plotted, with exposure to 16:0–5-doxyl PC at left (blue) or 16:0-14-doxyl PC at right (orange). The incomplete relaxation of L828-CG, I818-CD1, and K835-HN decays raise the question of some non-uniformity. Possibilities include dynamics, non-uniformity in their environments, or a subset of the bicelles lacking a spin-labeled probe.

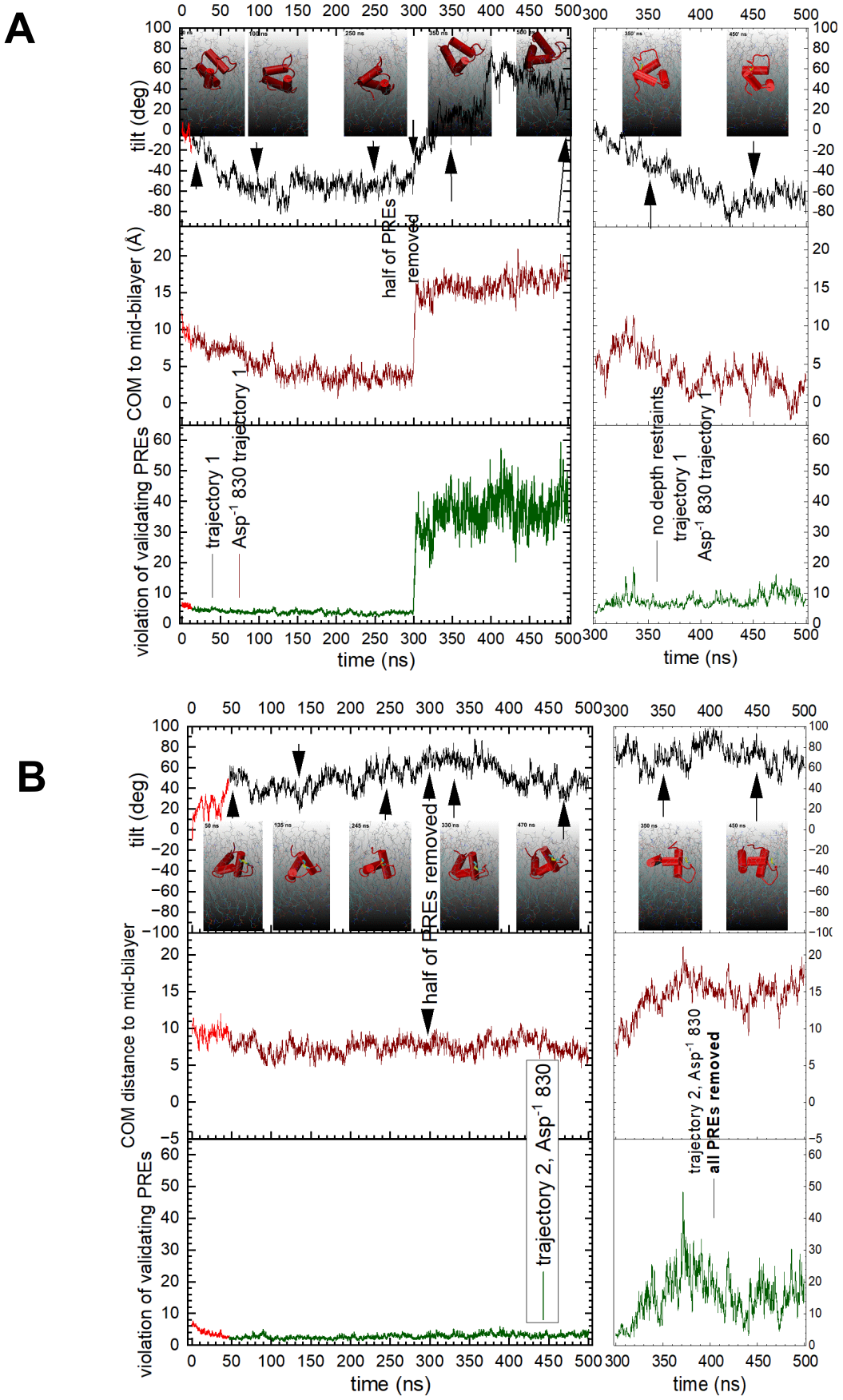

Figure S4. Change of tilt, depth, and consistency with validation set of PRE vs. time and upon withdrawal of half (middle) or all (right) of the depth restraints in the Asp^{-1} 830 simulations 1 and 2. Related to Fig. 5. Snapshots are plotted at about 100 ns intervals. Initial equilibration with NMR-derived restraints is marked by bright red.

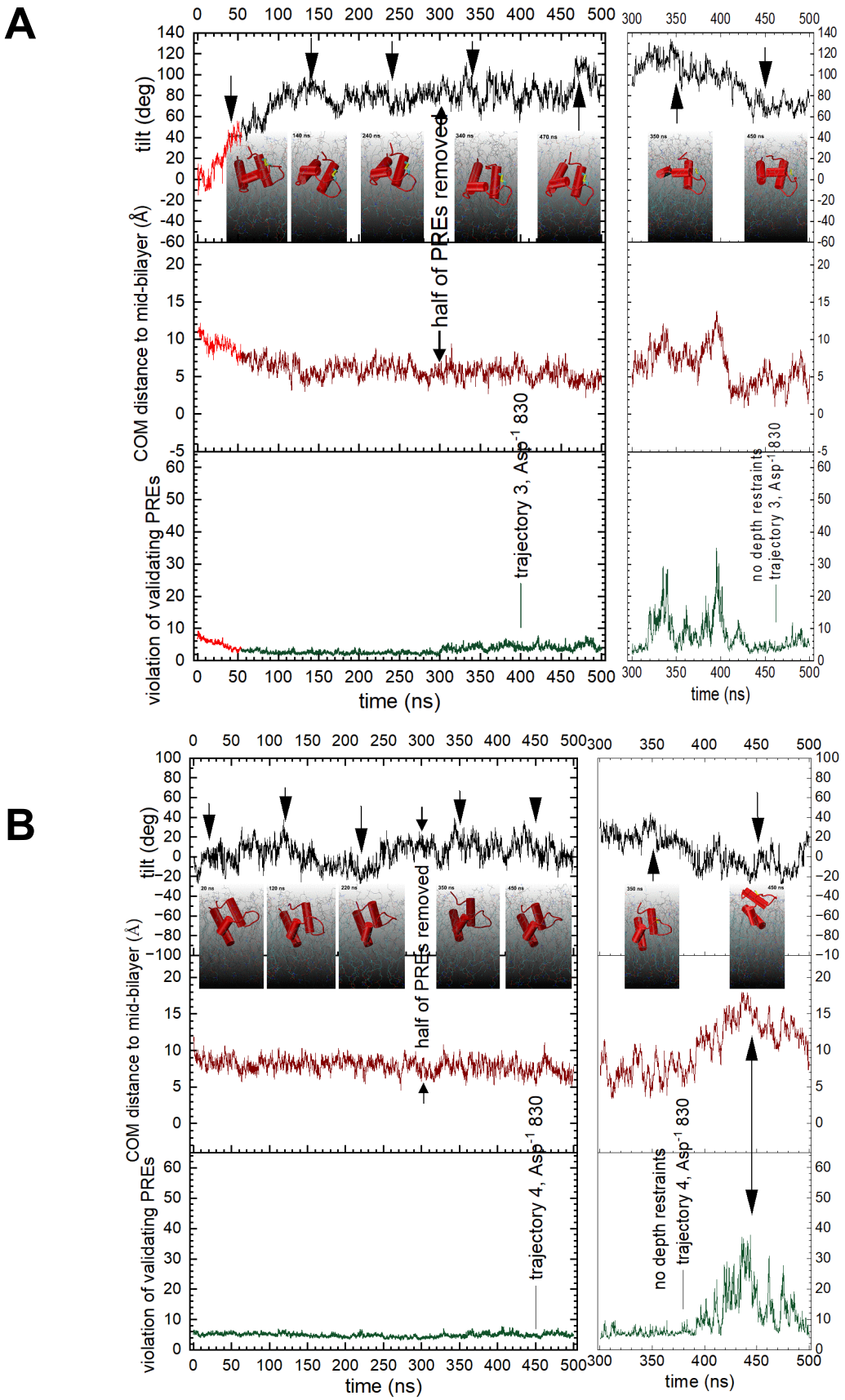

Figure S5. Change of tilt, depth, and consistency with validation set of PRE vs. time and upon withdrawal of half (middle) or all (right) of the depth restraints in the Asp^{-1} 830 simulations 3 and 4. Related to Fig. 5.

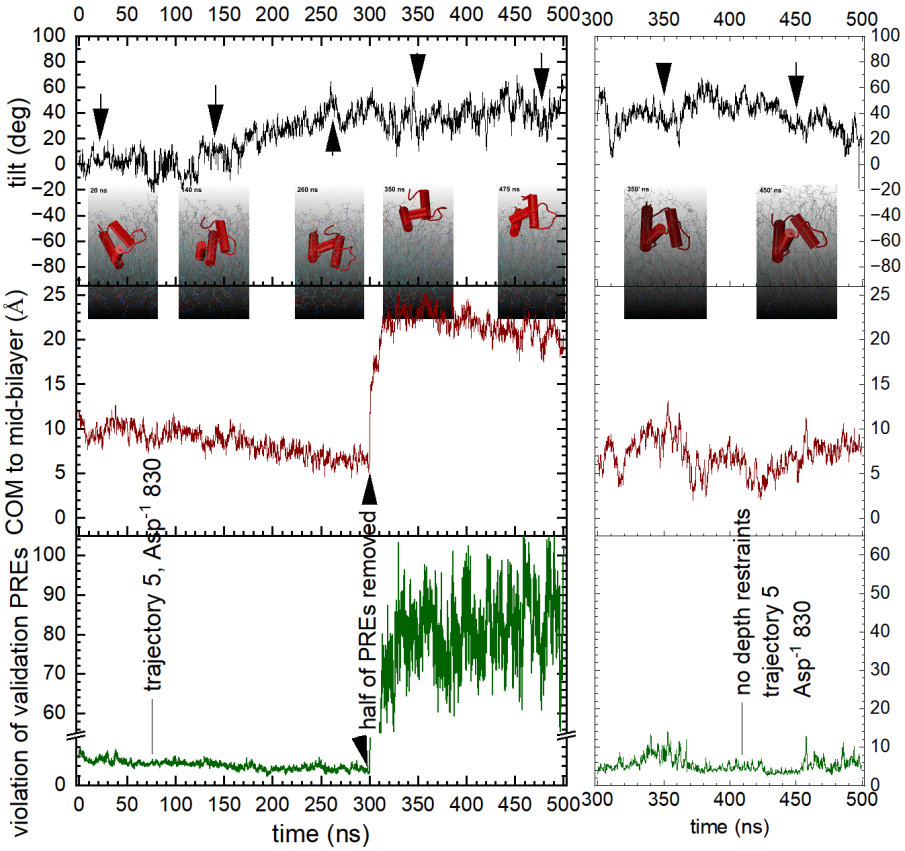

Figure S6. Change of tilt, depth, and consistency with validation set of PRE vs. time and upon withdrawal of half (middle) or all (right) of the depth restraints in the Asp^{-1} 830 simulation 5. Related to Fig. 5.

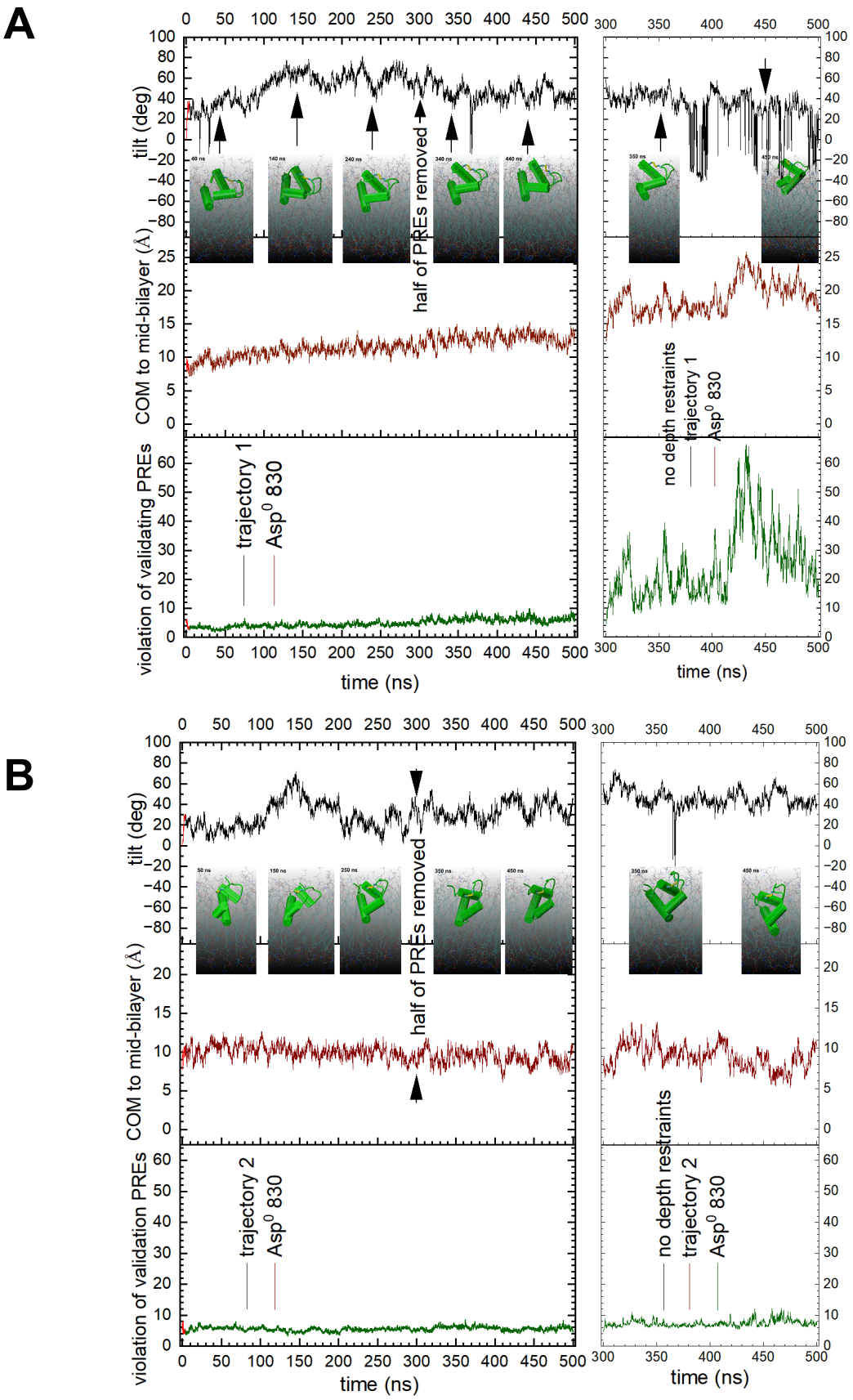

Figure S7. Change of tilt, depth, and consistency with validation set of PRE vs. time and upon withdrawal of half (middle) or all (right) of the depth restraints in the Asp^0 830 simulations 1 and 2. Related to Fig. 6.

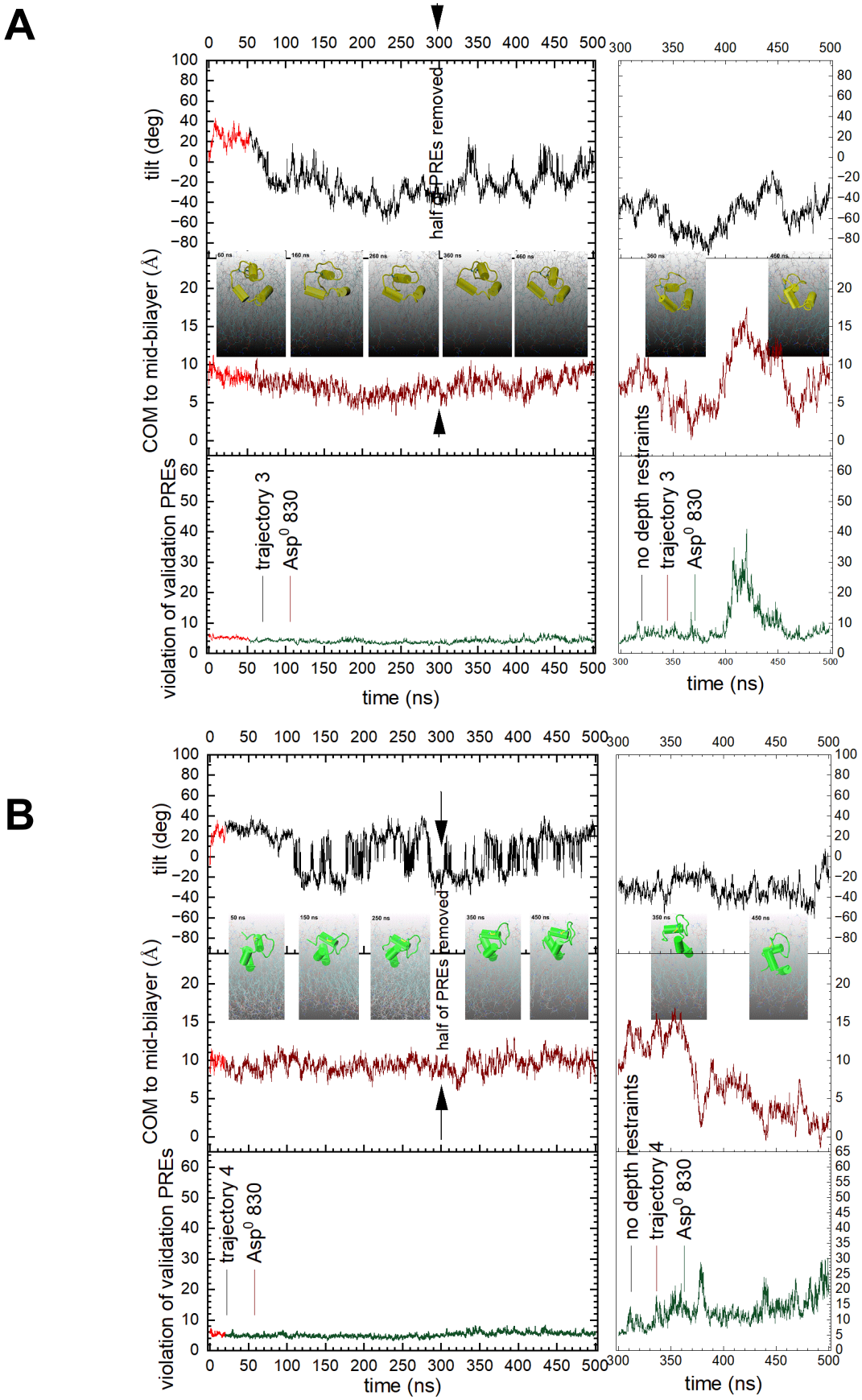

Figure S8. Change of tilt, depth, and consistency with validation set of PRE vs. time and upon withdrawal of half (middle) or all (right) of the depth restraints in the Asp^0 830 simulations 3 and 4. Related to Fig. 6.

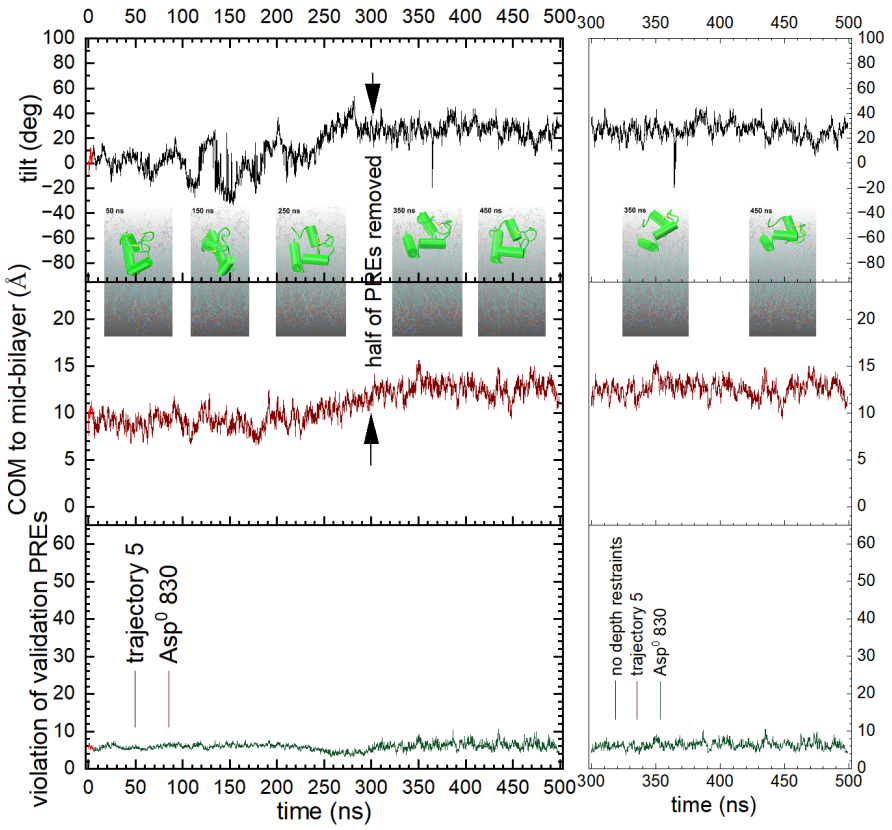

Figure S9. Change of tilt, depth, and consistency with validation set of PRE vs. time and upon withdrawal of half (middle) or all (right) of the depth restraints in the Asp^0 830 simulation 5. Related to Fig. 6.

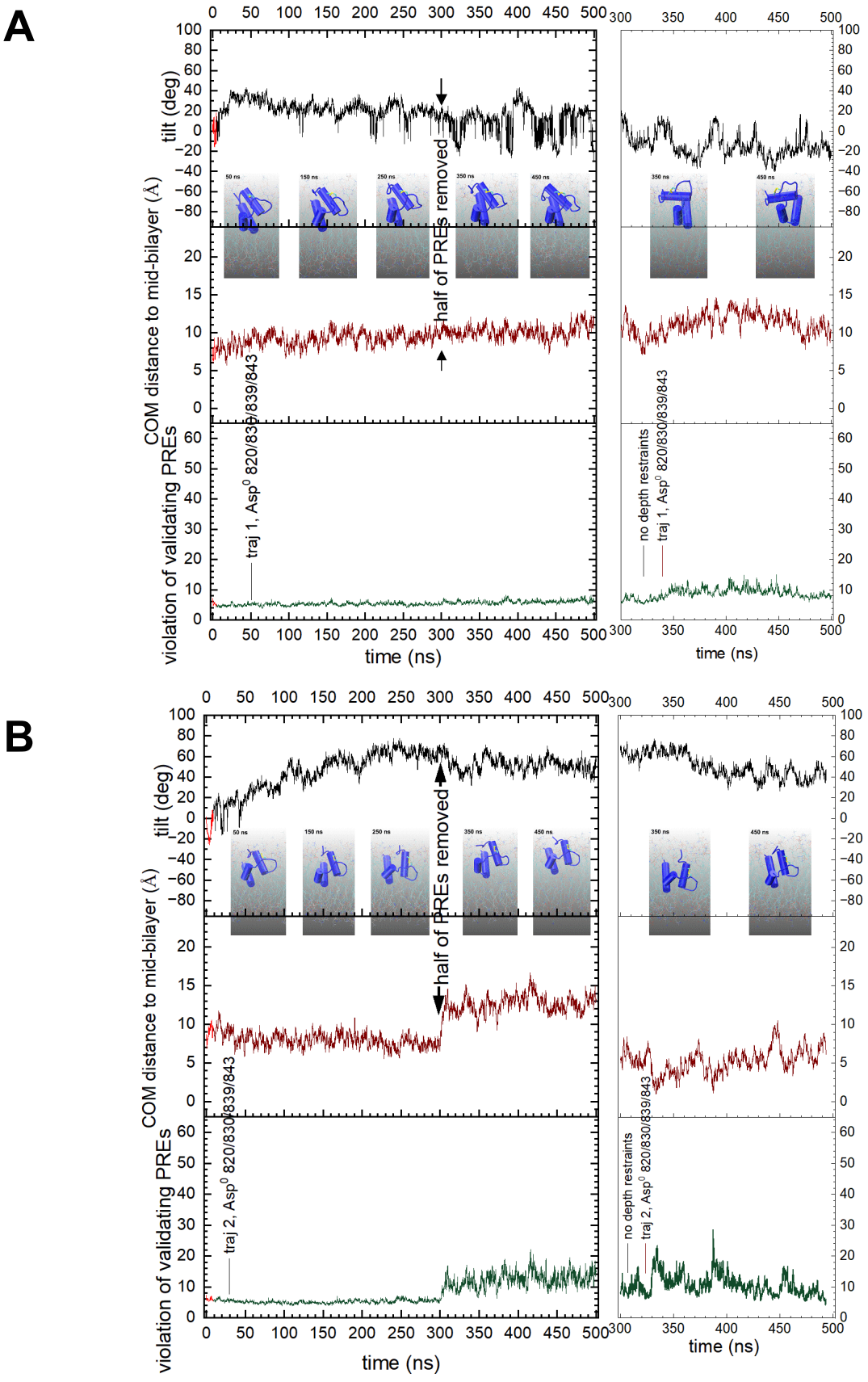

Figure S10. Change of tilt, depth, and consistency with validation set of PRE vs. time and upon withdrawal of half (middle) or all (right) of the depth restraints in simulations 1 and 2 of Asp^0 820/830/839/843. Related to Fig. 7.

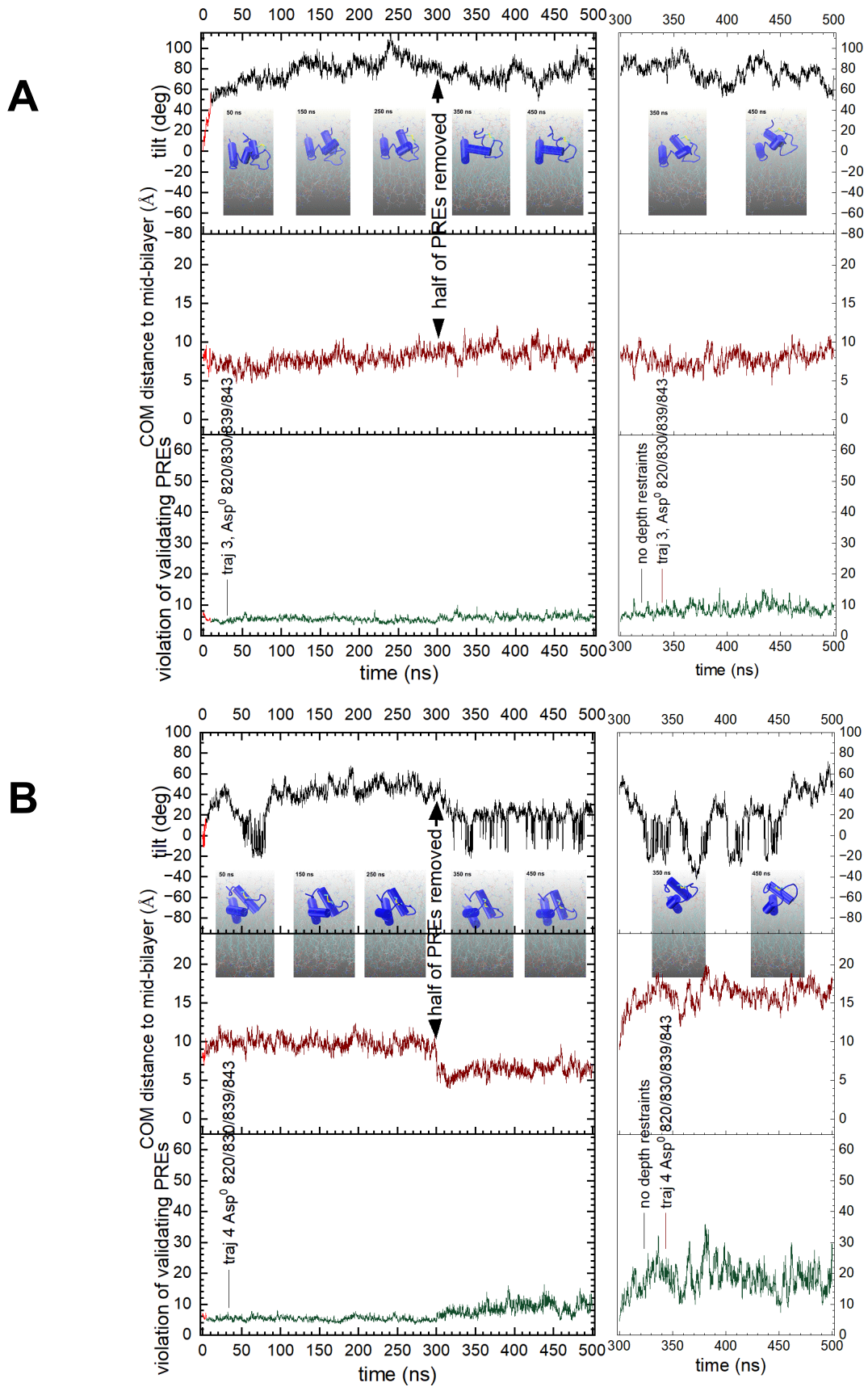

Figure S11. Change of tilt, depth, and consistency with validation set of PRE vs. time and upon withdrawal of half (middle) or all (right) of the depth restraints in simulations 3 and 4 of Asp^0 820/830/839/843. Related to Fig. 7.

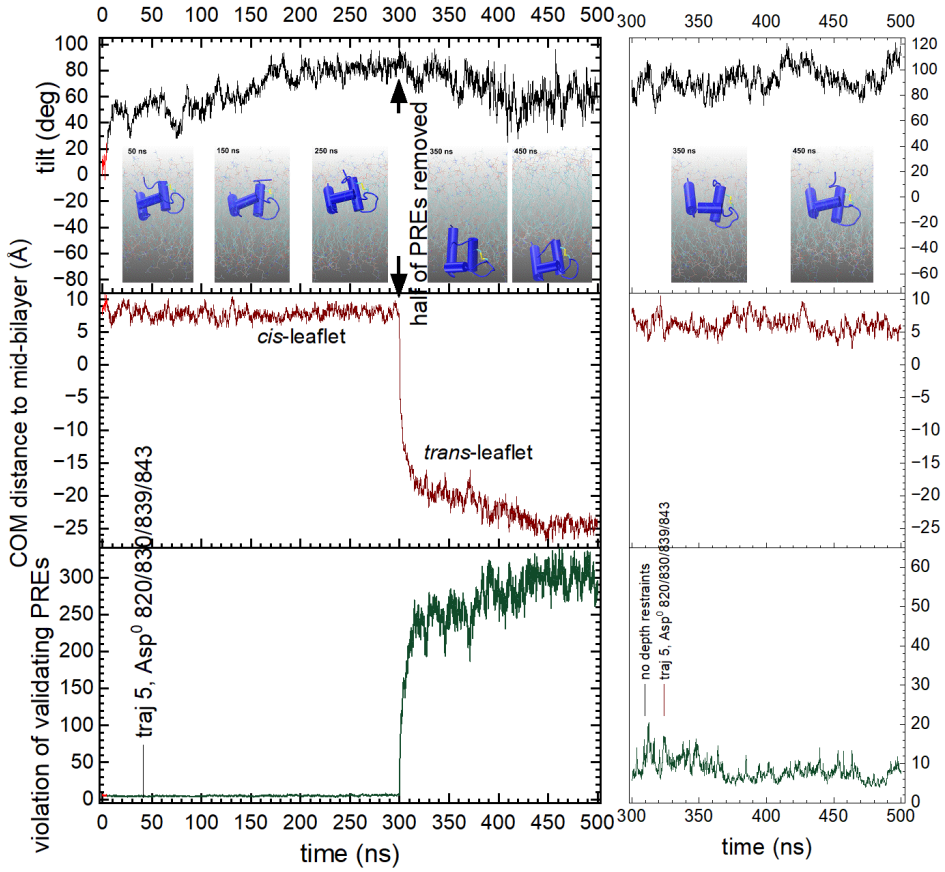

Figure S12. Change of tilt, depth, and consistency with validation set of PRE vs. time and upon withdrawal of half (middle) or all (right) of the depth restraints in simulation 5 of Asp^0 820/830/839/843. Related to Fig. 7.

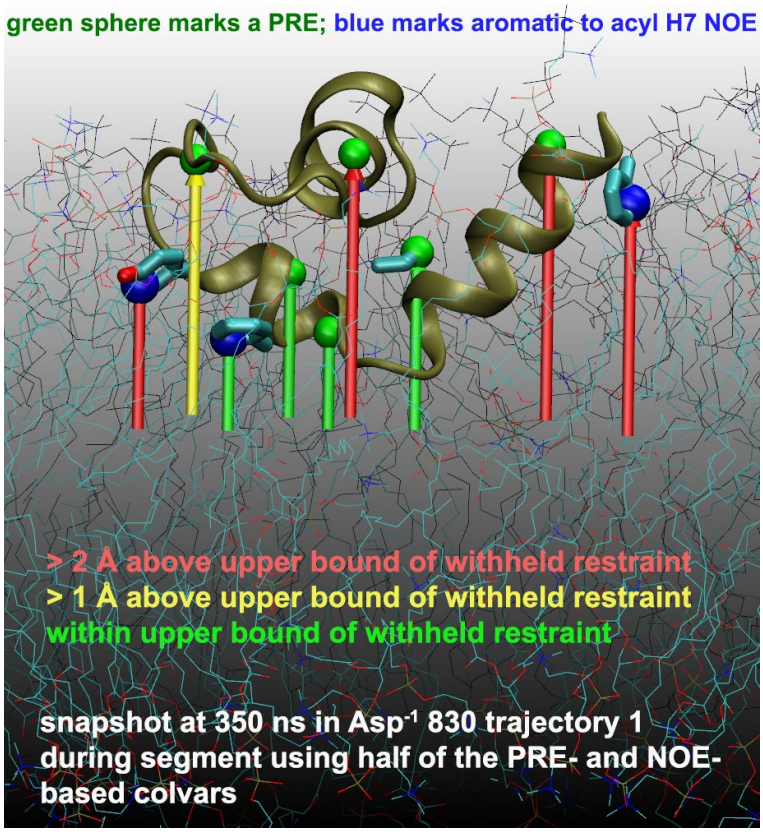

Figure S13. Examples of depth restraints with strategic consequences for positioning of FP within the DMPC bilayer. Related to Figures S4-S6. For comparison with NMR-estimated depths, simulated depths are plotted with rods at an illustrative instant in the portion of the Asp^{-1} 830 trajectory 1 restrained with half of the NMR estimates of depth. Nine of the 27 NMR-estimated depths withheld from this segment are represented. Five of these depths exceed their estimated upper bounds at this instant. When colvars such as these five were present in the simulations, they were likely to introduce gentle forces sufficient to discourage FP from visits this close to the aqueous phase.

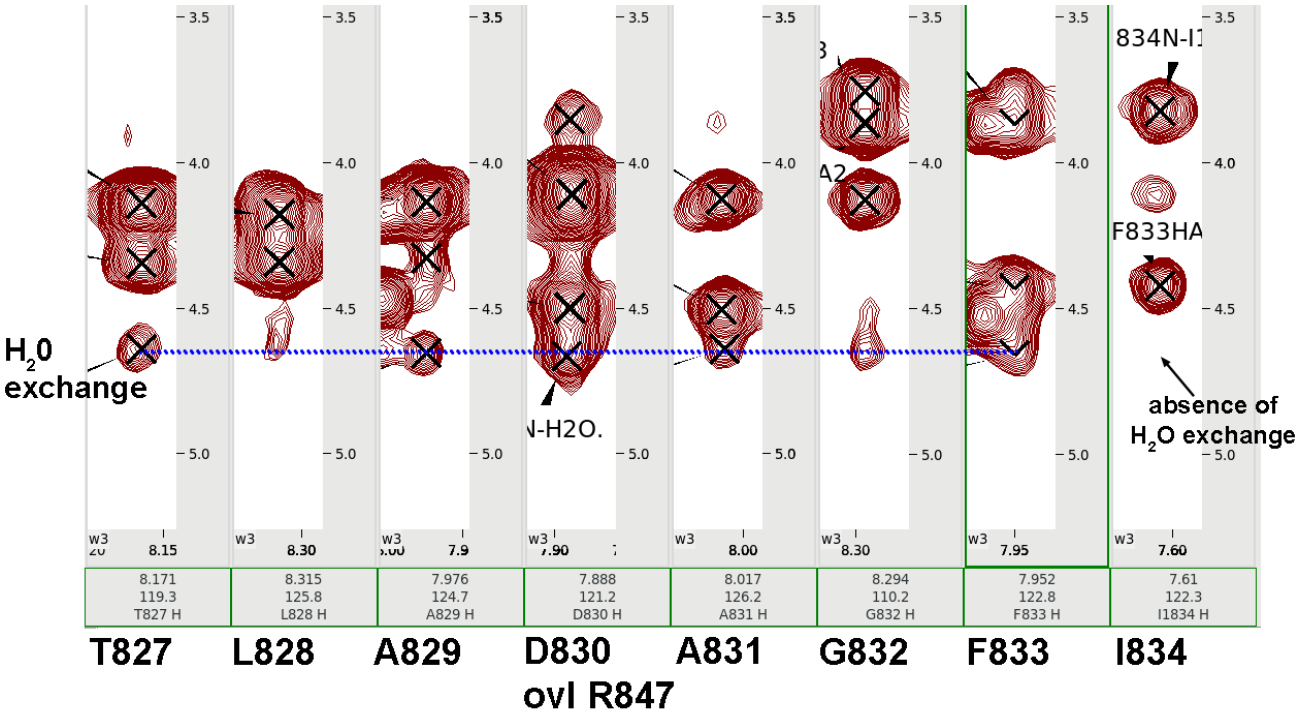

Figure S14. Water-amide exchange peaks from an ^{15}N-resolved NOESY spectrum of the SARS-CoV-2 fusion peptide in DMPC:DH^{7}PC bicelles at pH 5, 303K, and 800 MHz. Related to Figures 3, 5, and 6. The presence of the water exchange peaks suggests the water interactions of the backbone amide groups of Thr827 through Phe833, but not Ile834. The evidence for insertion of this region into the acyl phase of the membrane mimic is presented in Figures 2, 3, and S2 through S6.

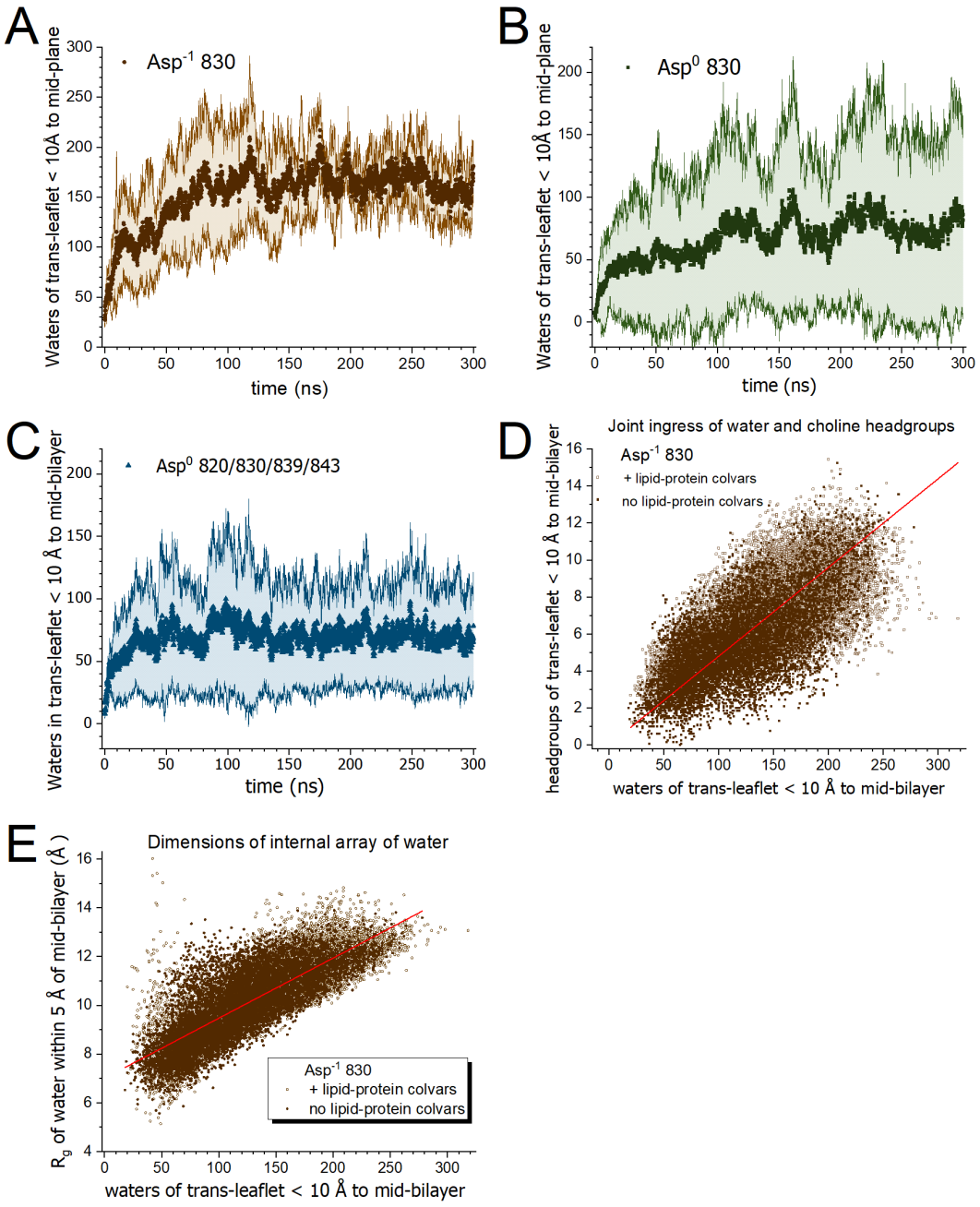

Figure S15. Gathering of water molecules across from the inserted SARS-CoV-2 fusion peptide in the interior 10 Å slab within the *trans*-leaflet of the DMPC bilayer. Related to Figures 3 and 4. Data for the ionization states with Asp^{-1} 830, Asp^{0} 830, and Asp^{0} 820/830/839/843 are plotted as mean and standard deviations across the sets of five replicated trajectories. Points represent snapshots every 100 ps. (A-C) The time courses of count the water molecules in the interior region of the *trans*-leaflet within 17 Å of the inserted fusion peptide domain in the NMR-biased MD simulations. The dark squares mark the mean count from the five trajectories in each condition. The lighter lines mark one standard deviation from the mean. (D) Using the five trajectories for Asp^{-1} 830, the counts of choline head groups and water molecules in the interior 10 Å slab of the *trans*-leaflet are correlated. (E) The radius of gyration, R_g, of the water molecules with ± 5 Å of the mid-plane of the bilayer is plotted against the count of water molecules in the interior 10 Å slab of *trans* leaflet from the five Asp^{-1} 830 trajectories. (D and E) add the points of the trailing 200 ns of simulations without NMR-based depth restraints (open symbols).

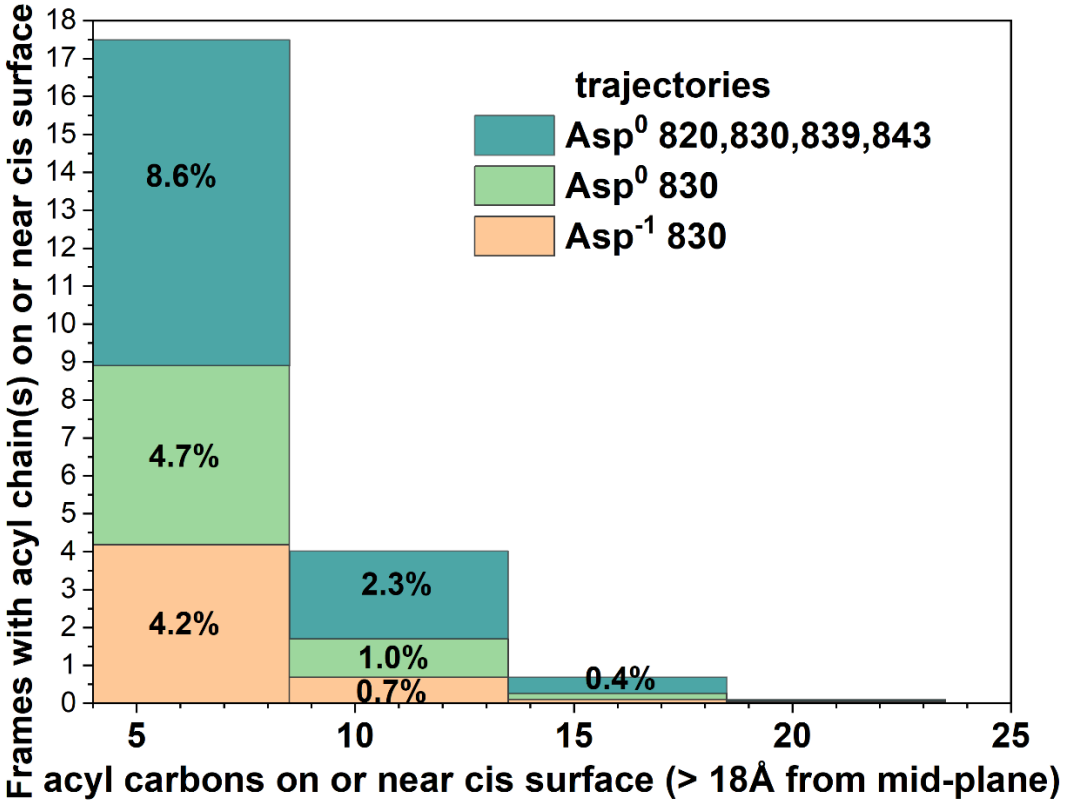

Figure S16. Fatty acyl groups rose to the surface of the *cis*-leaflet over FP in part of the Asp^0 820/830/839/843 trajectories. Related to Figures 3 and 4. Stacked histograms plot the frequency of lifting of 4 to 8, 9 to 13, 14 to 18, and 19 to 23 fatty acyl carbons to at least 18 Å from the mid-plane and near FP. The elevated fatty acyl chains appeared on the membrane surface on the *cis* side in Asp^0 820/830/839/843 simulations. In contrast, in the Asp^{-1} 830 and Asp^0 830 simulations, the affected phospholipid in its entirety was lifted, leaving the acyl chain mostly buried.

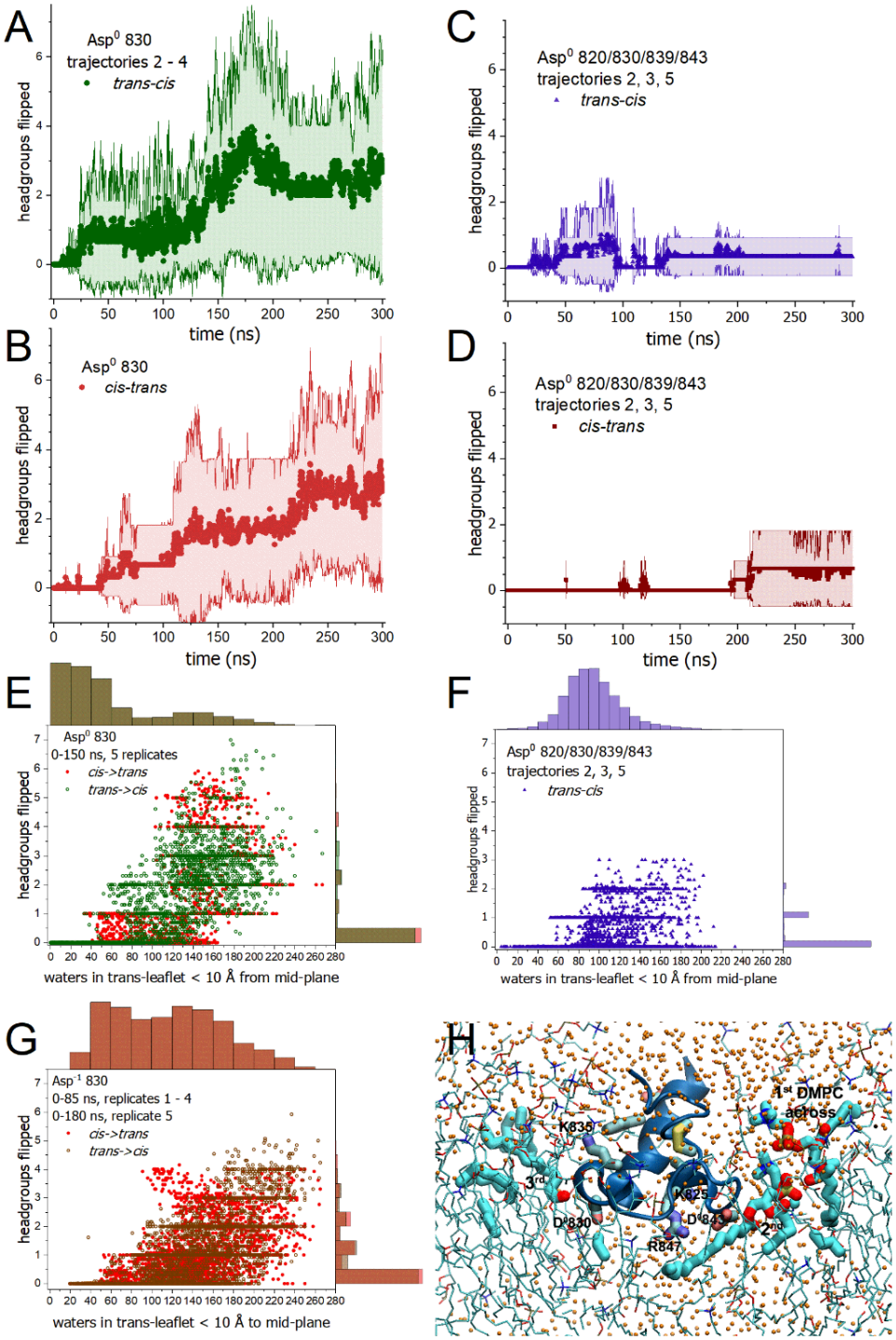

Figure S17. Flip-flop of DMPC with one or four Asp side chains protonated. Related to Fig. 8. Panels A and C plot the mean flip-flop from *trans*- to *cis*-leaflets. Panels B and D plot the mean flip-flop from cis- to *trans*-leaflets. The counts of headgroups flipped plotted vs. interior water in the *trans*-leaflet color the flip-flop from *trans*- to *cis*-leaflets green for Asp^0 830 (E) and purple for Asp^0 820/830/839/843 (F).The projections along the X- and Y-axes of E-G are plotted as histograms. (G) The headgroups flipped vs. interior water for the Asp^{-1} 830 condition is plotted for comparison. (H) The three DMPC molecules that flip-flopped into the *cis* leaflet of Asp^0 820/830/839/843 trajectory 5 are plotted with sticks. Key amino acid sidechains are plotted and labeled. Orange spheres mark water oxygen atoms.

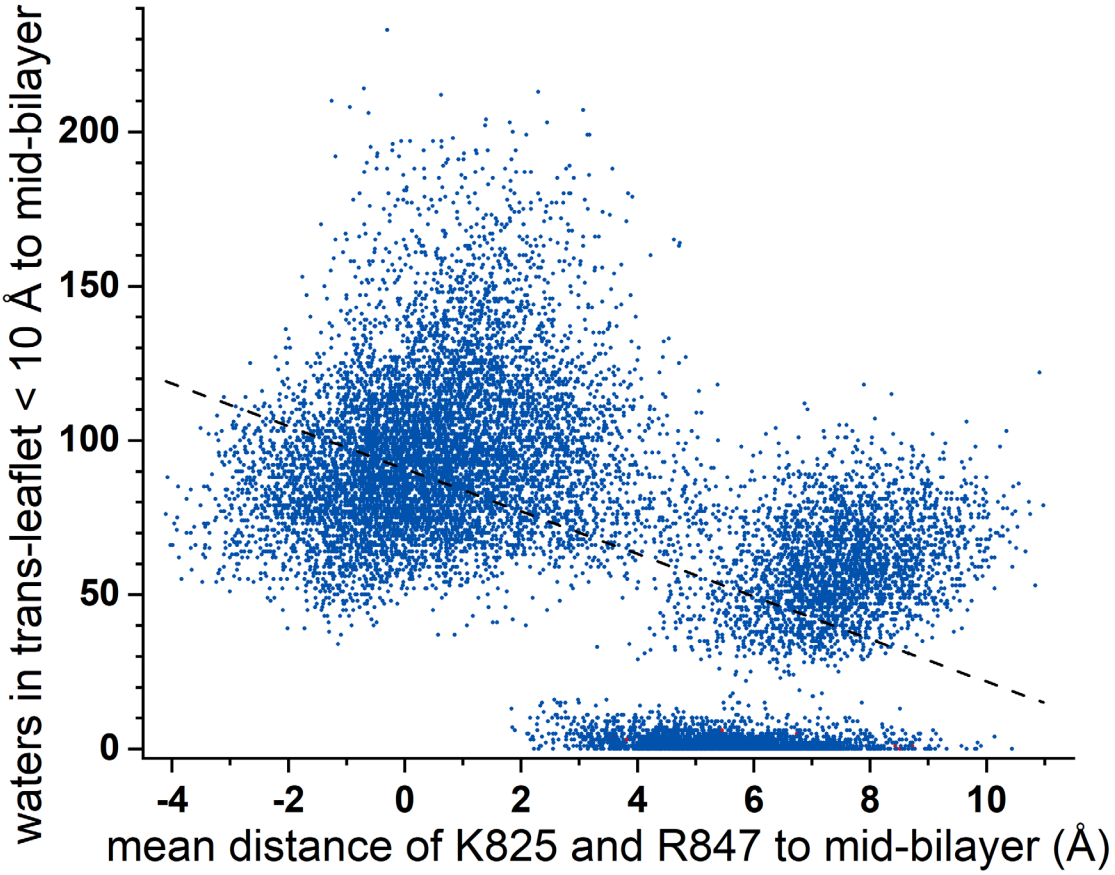

Figure S18. Relationship between ingress of water and positioning of Lys825 and Arg847 in the DMPC bilayer in the Asp^0 820/830/839/843 simulations. Related to Fig. 7. The number of water molecules counted in the trans-leaflet within 10 Å of the mid-plane of the DMPC bilayer is plotted against the mean distance of the basic groups of Lys825 and Arg847 to the mid-plane of the bilayer.

Table S1. Accession Numbers of Coronavirus Spike Sequences Aligned.[a]

Coronavirus	Accession number
α-coronaviruses	
CamelAlphaCoV	ALA50256
CCoV-1-71	AAV65515
CCoV-Elmo/02	AAP72149
FCoV-RM	ACT10854
HCoV-229E	AAK32188
HCoV-NL63	AGT51331
PEDV-CV777	AF353511_3
PRCV-ISU-1	ABG89317
TGEV-Miller-M6	ABG89301
TGEV-Purdue	CAB91145
FCoV-1683	AFH58021
β-coronaviruses	
Alpaca-BCoV	ABI93999
AnteCoV-US/OH1/2003	ABP38306
BCoV-Quebec	BAA00557
EquineCoV-NC99	AAQ67205
GiraCoV-US/OH3TC/2006	ABP38313
HCoV-HKU1	AAT98580
HCoV-OC43	AAX84791
MHV-A59	ACO72884
MHV-JHM	CAA28484
PHEV	AAL80031
BatCoV-273/2005	ABG47060
SARS-CoV	AAP13441
SARS-CoV-2	YP_009724390.1
BtRf-BetaCoV/HeB2013	AIA62290.1
SARS-CoV civet007	AAU04646.1
SARS-CoV-2 delta variant	UKA47815.1
BatCoV-133/2005	ABG47052
BatCoV-HKU4–1/2007	ABN10839
BatCoV-HKU5–1/2007	ABN10875
BatCoV-Neo/2011	AGY29650
BatCoV-PDF-2180	ARJ34226
BatCoV-SC2013/2013	AHY61337
EriCoV-VMC/DEU/2012	AGX27810
MERS-CoV-EMC/2012	AFS88936
MERS-CoV-HKU205	AHL18090
γ-coronaviruses	
BdCoV-HKU22	AHB63481
BeCoV-SW1	ABW87820
IBV-Beaudette	AAA70235
IBV-Cal99	AAS00080
IBV-M41	AAW33786
TCoV-MG10	ABW81427
AvCoV-gamma	ARJ35791.1
δ-coronaviruses	
BuCoV-HKU11	ACJ12044
MuCoV-HKU13	ACJ12062
ThCoV-HKU12	ACJ12053
PCoV-HKU15	AFD29187.1

[a] Related to Fig. 1E.

Table S2. Depth restraints from lipid-protein NOEs and PREs.[a]

Name + member, validation set	Protein atoms: numbers[b]	Acyl atom set[c]	Upper bound, Å	Force constant
F817HD – H7 NOE+	HD1,2: 23, 29	H7	5.0	0.02
F823HD – H2 NOE	HD1,2: 127, 133	H2	6.0	0.02
F833HD – H7 NOE+	HD1,2: 271, 277	H7	5.0	0.02
Y837HD – H7 NOE	HD1,2: 349, 356	H7	5.0	0.02
Y837HE – H7 NOE+	HE1,2: 351, 358	H7	5.0	0.02
L848HD – H2 NOE	HD11,12,13, 21, 22, 23: 401-403, 405-407	H2	6.0	0.02
I818Hn – 5-doxyl PRE	Hn: 35	H5	12.9	0.02
E819Hn – 5-doxyl PRE+	Hn: 54	H5	14.1	0.02
L821Hn – 5-doxyl PRE	Hn: 81	H5	14.4	0.02
N824Hn – 5-doxyl PRE+	Hn: 139	H5	14.0	0.02
K825Hn – 5-doxyl PRE	Hn: 153	H5	13.1	0.02
T827Hn – 5-doxyl PRE+	Hn: 191	H5	20.2	0.02
L828Hn – 5-doxyl PRE	Hn: 205	H5	19.3	0.02
A829Hn – 5-doxyl PRE+	Hn: 224	H5	17.9	0.02
G832Hn – 5-doxyl PRE	Hn: 256	H5	16.5	0.02
F833Hn – 5-doxyl PRE+	Hn: 263	H5	13.9	0.02
I834Hn – 5-doxyl PRE	Hn: 283	H5	14.4	0.02
K835Hn – 5-doxyl PRE+	Hn: 302	H5	13.3	0.02
Y837Hn – 5-doxyl PRE	Hn: 341	H5	13.5	0.02
G838Hn – 5-doxyl PRE+	Hn: 362	H5	13.3	0.02
C840Hn – 5-doxyl PRE	Hn: 381	H5	12.9	0.02
G842Hn – 5-doxyl PRE+	Hn: 410	H5	14.2	0.02
D843Hn – 5-doxyl PRE	Hn: 417	H5	12.9	0.02
L849Hn – 5-doxyl PRE+	Hn: 501	H5	13.4	0.02
I818HD – 5-doxyl PRE	HD1,2,3: 48-50	H5	19.1	0.02
I818G2 – 5-doxyl PRE+	HG21,22,23: 41-43	H5	19.4	0.02
D820HB – 5-doxyl PRE	HB1,2: 73, 74	H5	14.1	0.02
L821Ha – 5-doxyl PRE+	Ha: 83	H5	15.6	0.02
L822HB – 5-doxyl PRE	HB1,2: 104, 105	H5	14.9	0.02
L822HD – 5-doxyl PRE+	HD11, 12, 13, 21, 22, 23:109-111, 113-115	H5	20.0	0.02
F823HB – 5-doxyl PRE	HB1,2: 123, 124	H5	17.6	0.02
K825HB – 5-doxyl PRE+	HB1,2: 157, 158	H5	16.2	0.02
V826HB – 5-doxyl PRE	HB: 179	H5	18.9	0.02
F833HB – 5-doxyl PRE+	HB1,2: 267, 268	H5	15.3	0.02
I834HG1 – 5-doxyl PRE	HG1,2: 293, 294	H5	14.1	0.02
G838HA – 5-doxyl PRE+	HA1,2: 364, 365	H5	17.9	0.02
L841HB – 5-doxyl PRE	HB1,2: 395, 396	H5	16.2	0.02

V844HB – 5-doxyl PRE+	HB: 433	H5	13.7	0.02
L849HD – 5-doxyl PRE	HD11,12,13, 21,22,23: 510-512, 514-516	H5	15.5	0.02
E819Hn – 14-doxyl PRE+	Hn: 54	C14	16.0	0.02
T827Hn – 14-doxyl PRE	Hn: 191	C14	11.0	0.02
L828Hn – 14-doxyl PRE+	Hn: 205	C14	11.0	0.02
A829Hn – 14-doxyl PRE	Hn: 224	C14	11.0	0.02
G832Hn – 14-doxyl PRE+	Hn: 256	C14	13.1	0.02
F833Hn – 14-doxyl PRE	Hn: 263	C14	15.4	0.02
K835Hn – 14-doxyl PRE+	Hn: 302	C14	12.3	0.02
Y837Hn – 14-doxyl PRE	Hn: 341	C14	14.4	0.02
G838Hn – 14-doxyl PRE+	HN: 362	C14	13.8	0.02
V826HG – 14-doxyl PRE+	HG11,12,13, 21,22,23: 181-183, 185-187	C14	18.7	0.02
T827HG2 – 14-doxyl PRE	HG1,2,3: 199-201	C14	16.7	0.02
L828HG – 14-doxyl PRE+	HG: 212	C14	18.1	0.02
F833HB – 14-doxyl PRE	HB1,2: 267, 268	C14	19.1	0.02
I834HG1 –14-doxyl PRE+	HG1,2: 293, 294	C14	15.3	0.02
G842HA – 14-doxyl PRE	HA1,2: 412, 413	C14	17.9	0.02

[a] Related to Fig. 2 and Table 1.

[b] Atom numbering is given for the Asp^{-1} 830 state. Protonation of aspartate residues increments the atom indexes of the subsequent atoms in the list. Those numbering changes are listed in the .colvars restraint files deposited in https://osf.io/95tre/ entry “SARS2_fusion_peptide_in_membrane: NMR-biased_MD”.

[c] Atom numbers included in the respective atom acyl sets reflect the set of DMPC molecules specified https://osf.io/95tre/ in the step5_input.psf and .pdb files:

H7: 15682 15683 15719 15720 15800 15801 15837 15838 15918 15919 15955 15956 16036 16037 16073 16074 16154 16155 16191 16192 16272 16273 16309 16310 16390 16391 16427 16428 16508 16509 16545 16546 16626 16627 16663 16664 16744 16745 16781 16782 16862 16863 16899 16900 16980 16981 17017 17018

H2: 15658 15659 15667 15668 15776 15777 15785 15786 15894 15895 15903 15904 16012 16013 16021 16022 16130 16131 16139 16140 16248 16249 16257 16258 16366 16367 16375 16376 16484 16485 16493 16494 16602 16603 16611 16612 16720 16721 16729 16730 16838 16839 16847 16848 16956 16957 16965 16966

H5: 15676 15677 15794 15795 15912 15913 16030 16031 16148 16149 16266 16267 16384 16385 16502 16503 16620 16621 16738 16739 16856 16857 16974 16975

C14: 15702 15820 15938 16056 16174 16292 16410 16528 16646 16764 16882 17000 15938 17354 17472 18416 19006 19124 20304 20894 22782 23136 24198 24552 25260 25496 26204 27030 27974 28446

Table S3. NOE restraints within FP.[a]

NOE b	Upper bound, Å	Force constant, depth restraints present	Force constant, depth restraints absent
L849D1-L822G	5.0	0.05	0.01
L849D2-L822G	5.0	0.05	0.01
L849G-L822D1	5.0	0.05	0.01
L849G-L822D2	5.0	0.05	0.01
L849D-K825Hn	4.0	0.05	0.01
L849B-K825Hn	5.0	0.05	0.01
V826G-A831B	4.0	0.05	0.01
V826G-I834B	5.0	0.05	0.01
V826G-I850G1	5.0	0.05	0.01
A831B-I850G1	5.0	0.05	0.01
A831B-F855D	5.0	0.05	0.01
I834D-V844G	5.0	0.05	0.01
I834D-R847D1	5.0	0.05	0.01
I834D-R847D2	5.0	0.05	0.01
I834G2-R847G	5.0	0.05	0.01
L849D1-I834D	5.0	0.05	0.01
L849D2-I834D	5.0	0.05	0.01
L849D1-I834G2	5.0	0.05	0.01
L849D2-I834G2	5.0	0.05	0.01
V844G1-I850D	5.0	0.05	0.01
V844G2-I850D	5.0	0.05	0.01
V844G-I850G1	5.0	0.05	0.01
L849D-F855E	6.0	0.05	0.01
L849D-F855D	6.0	0.05	0.01
816A-818Hn	4.5	0.05	0.01
817A-819Hn	4.5	0.05	0.01
817A-820Hn	4.0	0.05	0.01
818Hn-820Hn	4.5	0.05	0.01
818A-820Hn	4.5	0.05	0.01
818A-821Hn	4.0	0.05	0.01
818A-822Hn	4.5	0.05	0.01
819A-821Hn	4.5	0.05	0.01
819A-822Hn	4.0	0.05	0.01
819A-823Hn	4.5	0.05	0.01
820A-822Hn	4.5	0.05	0.01
820A-823Hn	4.0	0.05	0.01
820A-824Hn	4.5	0.05	0.01
821A-823Hn	4.5	0.05	0.01
821A-824Hn	4.0	0.05	0.01
821A-825Hn	4.5	0.05	0.01
822A-824Hn	4.5	0.05	0.01
822A-826Hn	5.0	0.05	0.01
824A-826Hn	4.5	0.05	0.01
825A-827Hn	4.5	0.05	0.01
816B-818Hn	5.0	0.05	0.01
817D-821B	5.0	0.05	0.01
817D-821D1	5.0	0.05	0.01
817D-821D2	5.0	0.05	0.01
817E-821D1	5.0	0.05	0.01
817E-821D	5.0	0.05	0.01
818D-822D1	5.0	0.05	0.01
818D-822D2	5.0	0.05	0.01
818D-822G	5.0	0.05	0.01
818Hn-822D1	5.0	0.05	0.01
818Hn-822D2	5.0	0.05	0.01
818A-821D1	5.0	0.05	0.01
818A-821D2	5.0	0.05	0.01
822B-826Hn	5.0	0.05	0.01
822B-826G	5.0	0.05	0.01

822A-826G1	5.0	0.05	0.01
822A-826G2	5.0	0.05	0.01
822D-826G1	5.0	0.05	0.01
822D-826G2	5.0	0.05	0.01
823B1-825Hn	5.0	0.05	0.01
823B2-825Hn	5.0	0.05	0.01
825D-829Hn	5.0	0.05	0.01
826G1-829Hn	5.0	0.05	0.01
826G2-829Hn	5.0	0.05	0.01
826G-829B	5.0	0.05	0.01
826G1-830B	5.0	0.05	0.01
826G2-830B	5.0	0.05	0.01
827G-829Hn	5.0	0.05	0.01
827A-829Hn	5.0	0.05	0.01
827G-830Hn	5.0	0.05	0.01
827A-830Hn	5.0	0.05	0.01
829B-833D	5.0	0.05	0.01
833D-837D	5.0	0.05	0.01
831A-833Hn	4.5	0.05	0.01
831A-834Hn	4.0	0.05	0.01
831A-835Hn	4.5	0.05	0.01
832A-834Hn	4.5	0.05	0.01
832A-835Hn	4.0	0.05	0.01
833A-835Hn	4.5	0.05	0.01
833A-836Hn	4.0	0.05	0.01
833A-837Hn	4.5	0.05	0.01
834A-836Hn	4.5	0.05	0.01
844A-846Hn	4.5	0.05	0.01
844A–847Hn	4.5	0.05	0.01
846A-848Hn	4.5	0.05	0.01
849A-851Hn	4.5	0.05	0.01
851A-853Hn	4.5	0.05	0.01
851A-854Hn	4.0	0.05	0.01
853A-855Hn	4.5	0.05	0.01
853A-856Hn	4.0	0.05	0.01
854A-856Hn	4.5	0.05	0.01
845B-848Hn	5.0	0.05	0.002
845B-849Hn	5.0	0.05	0.002
846B-848Hn	5.0	0.05	0.002
846B-849Hn	5.0	0.05	0.002
847G-850G1	5.0	0.05	0.002
848Hn-852B	5.0	0.05	0.002
850D-852Hn	5.0	0.05	0.002
850D-853Hn	5.0	0.05	0.002
850A-853Hn	5.0	0.05	0.002
852B-855Hn	5.0	0.05	0.002
845Hn-846Hn	3.0	0.05	0.002
846Hn-847Hn	3.0	0.05	0.002
847Hn-848Hn	3.0	0.05	0.002
848Hn-849Hn	3.0	0.05	0.002
849Hn-850Hn	3.0	0.05	0.002
850Hn-851Hn	3.0	0.05	0.002
851Hn-852Hn	3.0	0.05	0.002
852Hn-853Hn	3.0	0.05	0.002
853Hn-854Hn	3.0	0.05	0.002
854Hn-855Hn	3.0	0.05	0.002
855Hn-856Hn	3.0	0.05	0.002
856Hn-857Hn	3.5	0.05	0.002

[a] Related to Table 1.

[b] Atom numbers are available in the .colvar files available at https://osf.io/95tre entry "SARS2_fusion_peptide_in_membrane: NMR-biased_MD"

Table S4. Sites of water interaction with backbone amide groups in FP inserted in bicelles: water exchange peaks in ^{15}N-separated NOESY at pH 5, 303K.[a]

Residue of FP, Spike numbering, helix number in FP	Amide-water exchange in ^{15}N-separated NOESY +: ≤ 7 peak contours ++ : 8-15 contours +++: ≥ 16 contours ovl: peak overlap	Residue of FP	Amide-water exchange in ^{15}N-separated NOESY
Ile818 in H1	+++, partial ovl Cys840	Asp839	no
Glu819 in H1	+	Cys840	+++, partial ovl Ile818
Asp820 in H1	no	Leu841	no
Leu821 in H1	no	Gly842	+
Leu822 in H1	no	Asp843	ovl with F855, +++
Phe823 in H1	ovl with Hα	Val844	no
Lys825 in H1	no	Ala845 in H3	++
Val826 in H1	no	Ala846 in H3	++
Thr827	++	Arg847 in H3	ovl with D830, +++
Leu828	++	Asp848 in H3	++
Ala829	++	Leu849 in H3	+
Asp830	ovl with R847, +++	Ile850 in H3	no
Ala831 in H2	++	Cys851 in H3	no
Gly832 in H2	++	Ala852 in H3	no
Phe833 in H2	++	Gln853 in H3	+++
Ile834 in H2	no	Lys854	+++
Lys835 in H2	no	Phe855	ovl with D843, +++
Gln836 in H2	no	Asn856	ovl with Hα
Tyr837 in H2	+	Gly857	ovl with Hα
Gly838	++		

[a] Related to Fig. 3.